Distributed Load-Side Control: Coping with Variation of Renewable Generations

Zhaojian Wang, Feng Liu, Steven H. Low, Peng Yang and Shengwei Mei

***Abstract*—This paper addresses the distributed load frequency control of multi-area power system, where controllable loads are utilized to recover nominal frequencies for the advantage of fast response speed. The imbalanced power causing frequency deviation is decomposed into three parts: a known constant part, an unknown low-frequency variation part and a high-frequency residual. The known steady part is usually the prediction of power imbalance. The variation may result from the fluctuation of renewable resources, electric vehicle charging, etc., which is usually unknown to operators. The high-frequency residual is usually unknown and treated as an external disturbance. Correspondingly, in this paper, we resolve the following three problems in different timescales: 1) allocate the steady part of power imbalance economically; 2) mitigate the effect of unknown low-frequency power variation locally; 3) attenuate unknown high-frequency disturbances. To this end, a distributed controller combining consensus method with adaptive internal model control is proposed. We first prove that the closed-loop system is asymptotically stable and converges to the optimal solution of an optimization counterpart problem if the external disturbance is not included. We then prove that the power variation can be mitigated accurately. Furthermore, we show the closed-loop system is robust against both parameter uncertainty and external disturbances. The New England system is used to verifiy the efficacy of our design.**

***Index Terms*—Load-side control, renewable generation, internal model control; frequency regulation; distributed control.**

I. Introduction

A. Background

In the modern power system, multiple regional grids are usually interconnected to constitute a bulk grid [1], [2]. To maintain a stable power system, the frequency should be retained at its nominal value, e.g. 50Hz or 60Hz. Conventionally, it is realized by synchronized generators in a centralized fashion, known as a hierarchy control architecture [3], [4]. However, with the increasing penetration of volatile and uncertain renewable generations, power mismatch in the system can fluctuate rapidly with a large amount. In such a situation, the traditional manner of control may not be able to keep pace due to large inertia of traditional synchronous generators. Fortunately, load-side participation in frequency control opens up new possibility to resolve this problem, benefiting from its fast response [5], [6]. On the other hand, as controllable loads usually disperse across the power system, it is desired to fit load-side control into a distributed architecture rather than the conventional centralized one. In this regard, distributed optimal control has been investigated by connecting the controller design with solving algorithms of optimal dispatch problems [7]–[9]. It leads to a so-called *reverse engineering* methodology for designing optimal controllers, particularly in optimal frequency control of power systems [6], [10], [11]. In this paper, we design a distributed load-side frequency controller that is capable of adapting to power variation due to high-penetration volatile renewable generations, such as wind farms and PV clusters.

This work was supported by the National Natural Science Foundation of China (No. 51677100, No. 51377092, No. 51621065), the US National Science Foundation through awards EPCN 1619352, CCF 1637598, CNS 1545096, ARPA-E award DE-AR0000699, and Skoltech through Collaboration Agreement 1075-MRA. (Corresponding author: Shengwei Mei)

Z. Wang, F. Liu, P. Yang and S. Mei are with the State Key Laboratory of Power System and Department of Electrical Engineering, Tsinghua University, Beijing, China, 100084 e-mail: (meishengwei@mail.tsinghua.edu.cn).

S. H. Low is with the Department of Electrical Engineering, California Institute of Technology, Pasadena, CA, USA, 91105 e-mail:(slow@caltech.edu)

B. Related Work

In power system operation, frequency deviation is usually a consequence of power mismatch due to unexpected disturbances, such as sudden load leaping/dropping or generator tripping. In terms of the forms of imbalanced power, these state-of-the-art works can be roughly divided into two categories: constant power imbalance [6], [12]–[17] and time-varying power imbalance [18]–[20]. In the first category, a step change of load/generation is considered. Then generators and/or controllable loads are utilized to eliminate the imbalanced power and restore the nominal frequency. In [6], an optimal load-side control problem is formulated and a primary frequency controller is derived to balance step power change using controllable loads. It is extended in [12] to realize a secondary frequency control, i.e. restoring the nominal frequency. The design approach is generalized in [14], where the model requirement is relaxed and a passivity condition is proposed to guarantee the asymptotic stability. [15], [16] further consider both steady-state and transient operational constraints in distributed optimal frequency control. In [13], a nonlinear network-preserving model is considered and only limited control coverage is needed to implement the distributed optimal frequency control. A different disturbance is considered in [17], where th secondary frequency controller is injected by constant malicious attacks. To eliminate the influence of the attacks, a detection method is derived to combine with the distributed frequency controller.

In the second category, imbalanced power does not keep constant, creating much greater challenge to controller design and stability analysis. In [18], power variation is modeled as output of a known exosystem. Then an internal model controller is designed to tackle and compensate the time-varying imbalanced power. The idea of combining distributed

control awith internal model control is attractive and inspiring. In [19], a centralized controller is proposed, which can well track the power imbalance and maintain the global frequency within a desired range when considering slowly changing power imbalance. The frequency still varies along with time-varying loads. In [20], measurement noise is considered in frequency control, and a leaky integral controller is proposed that can strike an acceptable trade-off between performance and robustness.

To sum up, in most of the existing literature, imbalanced power is modeled as a step change, implying it can be regarded a constant almost everywhere. The time-varying imbalanced power is usually regarded as output of a *known* exosystem. However, these two kinds of power imbalance are not in accordance with the practice in power systems, especially when a large amount of renewable generations and electric vehicles are integrated. In such a situation, power imbalance is always time-varying and unknown, which should be carefully considered in the design of distributed frequency control.

C. Contribution

In this paper, imbalanced power is modeled in a more realistic fashion. It is decomposed into a known constant part, an unknown low-frequency time-varying part and a high-frequency residual. In power systems, the first one can be obtained by prediction while the latter two are the fluctuation around the prediction. Offset error in prediction can also be considered in the unknown time-varying part. Then, we give a systematic way to deal with the time-varying disturbance. First, a distributed control is proposed based on consensus method to balance the known constant part economically, which resolves a slow timescale operation problem. Second, a decentralized supplementary controller based on the internal model control is proposed to mitigate the effect of unknown power variation, which deals with low-frequency variation in a faster timescale. Finally, we also investigate that the proposed controller can attenuate the impact of high-frequency residual, which is in the fastest timescale.

This work can be regarded as an extension of [6], [12]–[16]. As the imbalanced power is time varying in our case, these previous distributed controller may not be able to stabilize and restore the frequency, as we will demonstrate later in case studies. Here the main challenge is how to fit a time-varying tracking and compensation control into the structure of the previous distributed frequency controller. The major difference between this paper and [18] is that the power variation is modeled as output of a known exosystem in [18]. Since such information is difficult to obtain in practice, our model appears to be more practical albeit more sophisticated. In [21], an internal model control is leveraged to devise a distributed *unconstrained* optimization which can mitigate the effects of unknown time-varying disturbances. In contrast, we consider optimal frequency control problem with both *power system dynamics* as well as *power balance constraints*, which are not included in [21]. Moreover, we also analyze the robustness of the proposed controller under uncertain parameters and disturbances, which has been seldom discussed in the distributed frequency control literature. Main contributions of this paper are as follows:

- A generic model of imbalanced power for power system frequency control is established, which is composed of three parts: a known constant part, a unknown low-frequency power variation part and a high-frequency residual. The power variation is further modeled by a superposition of several dominant sinusoidal components. Then it is formulated as the output of an exosystem with unknown parameters;
- A distributed controller is derive to restore the nominal frequency even under unknown disturbance. It is composed of two parts. One is designed based on consensus control to achieve an economic allocation of the constant part of power imbalance, while the other is designed based on adaptive internal model control to mitigate the effect of unknown power variation;
- Robustness of the controller under parameter uncertainty and external disturbances is analyzed. It is proved that the influence of uncertain damping constants have no impact on the performance of the controller and the impact of external disturbances is attenuated greatly.

D. Organization

The rest of this paper is organized as follows. In Section II, the network and imbalanced power models are formulated, respectively. Section III presents the design of distributed frequency controller. In Section IV, the equilibrium of the closed-loop system is characterized with a proof of asymptotic stability. The robustness of the proposed controller under uncertainties is analyzed in Section V. We confirm the performance of controllers via simulations on a detailed power system model in Section VI. Section VII concludes the paper.

II. Problem Formulation

A. Model of Power Network

A large power network is usually composed of multiple control areas, which are interconnected with each other through tie lines. For simplicity, here we treat each control area as a node with an aggregate controllable load and an aggregate uncontrollable power injection.[1] Then the power network is modeled as a graph $\mathscr{G} := (N, E)$ where $N = \{1, 2, ...n\}$ is the set of nodes (control areas) and $E \subseteq N \times N$ is the set of edges (tie lines). If a pair of nodes i and j are connected by a tie line directly, we denote the tie line by $(i, j) \in E$. $\mathscr{G}$ is treated as directed with an arbitrary orientation and we use $(i, j) \in E$ or $i \to j$ interchangeably to denote a directed edge from i to j. Without loss of generality, we assume $\mathscr{G}$ is connected.

Besides the graph of physical power network, we also need to consider the communication network, denoted by $\mathscr{H}$. A edge in $\mathscr{H}$ stands for that the two endpoints of the edge can communicate to eahc other directly. Whereas the nodes in the two networks are identical, their edges can be different. In this

[1] In our study, all controllable loads in the same area are aggregated into one controllable load. The same as the aggregate uncontrollable power injection. This simplification is practically reasonable when dealing with the frequency control problem in power systems [10].

paper, we assume $\mathscr{H}$ is also connected. The set of neighbors of node j in the communication graph is denoted by N_{cj}. The Laplacian matrix of $\mathscr{H}$ is denoted as L.

A second-order linearized model is adopted to describe the frequency dynamics of each node. We assume the tie lines are lossless and adopt the DC power flow model, which is reasonable for a high-voltage transmission system. Then for each node $j \in N$, we have

$$\begin{aligned} \dot{\theta}_j &= \omega_j && \text{(1a)} \\ M_j\dot{\omega}_j &= P_j^{in} - P_j^l - D_j\omega_j \\ &\quad + \sum_{i:i\to j} B_{ij}(\theta_i-\theta_j) - \sum_{k:j\to k} B_{jk}(\theta_j-\theta_k) && \text{(1b)} \end{aligned}$$

where, θ_j denotes the rotor angle at node j; ω_j the frequency; P_j^{in} the uncontrollable power injection; P_j^l the controllable load. $M_j > 0$, $D_j > 0$ are inertia and damping constants, respectively. $B_{jk} > 0$ are line parameters that depend on the reactance of line $(j,k) \in E$.

B. Model of Imbalanced Power

Denote P_j^{in} as the imbalanced power in the system. It can be decomposed into two parts: a constant part and a variation part. That is

$$P_j^{in}(t) = \overline{P}_j^{in} + \tilde{q}_j(t) \quad (2)$$

where $\overline{P}_j^{in}$ is the known constant part, which could be the prediction of renewable generations and/or loads. $\tilde{q}_j(t)$ is the variation part, which is assumed unknown.[2]

The known constant part is easy to deal with, while the variation part is non-trivial. The main idea is to further decompose it into the sum of a series of sinusoidal functions, whose parameters are unknown. Then an internal model control can be utilized to trace these sinusoidal components, and then eliminate the effects of the variation part.

In light of [22]–[24], we can approximate variation of renewable generations and load demands by a superposition of a few sinusoidal functions. Specifically, we decompose the imbalanced power injected by volatile renewable generation and loads $\tilde{q}_j(t)$ into

$$\tilde{q}_j(t) := q_{j0} + \sum_{k=1}^{s_j} q_{jk}\sin(a_{jk}\cdot t + \phi_{jk}) + w_j(t) \quad (3)$$

where q_{j0} is the prediction offset error (which is an unknown constant). The second term stands for the variation part, which is a superposition of a few sinusoidal functions. s_j is the number of sinusoidal functions for node j. Their amplitudes (i.e. q_{jk}), frequencies (i.e. $a_{jk} > 0$) and initial phases (i.e. ϕ_{jk}) are unknown but belong to a known bounded interval. Note that it is practically impossible to use infinite number of sinusoidal signals to represent $\tilde{q}_j(t)$. Hence here we consider only several dominant frequencies (usually few low-frequency power fluctuations). The remained high-frequency residuals, denoted by $w_j(t)$, is usually quite small. So we do not consider its detailed model in this paper, but simply assume that it belongs to the $\mathscr{L}_2^T$ space, i.e., for any $w_j(t)$ $(j \in N)$, $\int_0^T ||w_j(t)||^2 \mathrm{d}t < +\infty$ holds for all $0 < T < +\infty$. In this way, $w_j(t)$ is treated as an external disturbance.

[2] As $\overline{P}_j^{in}$ may not be accurate, the offset error of prediction is included in $\tilde{q}_j(t)$ component. We abuse the term $\tilde{q}_j(t)$ "variation part" for simplicity.

Remark 1 (Power Variation in power system)**.** In this paper, we adopt a generic model to depict $\tilde{q}_j(t)$ so that it can apply for various types of power imbalance in practice. In practical power systems, $\tilde{q}_j(t)$ has many interpretations, some of which are listed below.

1) Variation of renewable generations. Large-scale renewable generations may vary rapidly, causing remarkable power fluctuation. As it is difficult to accurately predict volatile renewable generations, the fluctuation is always partly unknown. Such unknown variations may lead to remarkable frequency fluctuation or even instability.
2) Variation of loads. Load demands in a power system are always varying, which also bring out power fluctuation in system. In addition, whereas load demand usually can be estimated quite accurately in a traditional power system. However, the integration of electric vehicles, energy storage and demand response has been making load demands much more difficult to predict.

C. Equivalent Transformation of Disturbance Model

We further investigate the dominant part in $\tilde{q}_j(t)$. Denote

$$q_j(t) := q_{j0} + \textstyle\sum_{k=1}^{s_j} q_{jk}\sin(a_{jk}\cdot t + \phi_{jk}) \quad (4)$$

Then we show that $q_j(t)$ can be expressed as the output of an exosystem. To this end, define

$$\begin{aligned} \lambda_{j1} &= q_j(t) \\ \lambda_{jk} &= \left(\frac{\mathrm{d}}{\mathrm{d}t}\right)^{k-1} q_j(t) \quad (2 \le k \le \bar{s}_j) && \text{(5)} \end{aligned}$$

where $\bar{s}_j := 2s_j + 1$. Then $q_j(t)$ is just the output of the following dynamic system [21], [25]:

$$\begin{aligned} \dot{\lambda}_j &= A_j(\alpha_j)\lambda_j && \text{(6a)} \\ q_j(t) &= [1\ \mathbf{0}_{1\times 2s_j}]\cdot\lambda_j && \text{(6b)} \end{aligned}$$

where,

$$\begin{aligned} \lambda_j &:= [\lambda_{j1},\cdots,\lambda_{j,\bar{s}_j}]^T \\ A_j(\alpha_j) &:= \begin{bmatrix} \mathbf{0}_{2s_j\times 1} & I_{2s_j} \\ 0 & \alpha_{j1},0,\cdots,\alpha_{js_j},0 \end{bmatrix} && \text{(7)} \end{aligned}$$

with $\alpha_{j1} = -\prod_{l=1}^{s_j} a_{jl}^2$, $\alpha_{j2} = -\sum_{k=1}^{s_j}\prod_{\substack{l=1\\ l\neq k}}^{s_j} a_{jl}^2$, $\cdots$, $\alpha_{js_j} = -\sum_{l=1}^{s_j} a_{jl}^2$. Here, a_{jl} are defined in (4).

To facilitate the controller design, a transformation is constructed. Let $R_j := [r_{i1},\cdots,r_{i,\bar{s}_j-1},1]$, such that all the roots of polynomial $\tau^{\bar{s}_j-1} + r_{i,\bar{s}_j-1}\tau^{\bar{s}_j-2} + \cdots + r_{i2}\tau + r_{i1}$ have negative real parts. Then define a vector $\tilde{A}_j(\alpha_j) := R_j(I_{\bar{s}_j} + A_j(\alpha_j))$ and construct the following matrix

$$O_j(\alpha_j) := \left[\tilde{A}_j^T(\alpha_j),\cdots,\left(\tilde{A}_j(\alpha_j)A_j^{\bar{s}_j-1}(\alpha_j)\right)^T\right]^T$$

In [26] , it is proven that $O_j(\alpha_j)$ is nonsingular, and

$$O_j^{-1}(\alpha_j)A_j(\alpha_j)O_j(\alpha_j) = A_j(\alpha_j)$$

Let $\varphi_j = O_j^{-1}(\alpha_j)\lambda_j$, then we have

$$\begin{aligned} \dot{\varphi}_j &= A_j(\alpha_j)\varphi_j && \text{(8a)} \\ q_j(t) &= \tilde{A}_j(\alpha_j)\varphi_j && \text{(8b)} \end{aligned}$$

So far, $q_j(t)$ is written as the output of a new exosystem (8a). However, Elements in $A_j(\alpha_j)$ and $\tilde{A}_j(\alpha_j)$ are still unknown. According to the definition of $q_j(t)$ and boundedness of q_{jk}, a_{jk}, λ_j is bounded. Hence φ_j is also bounded due to the nonsingular transformation.

From (2), (3) and (4), $P_j^{in}(t)$ is composed of three parts, i.e., $\overline{P}_j^{in}$, $q_j(t)$ and $w_j(t)$, we will address them in different ways, giving rise to the following three problems.

P1: Balancing $\overline{P}_j^{in}$ economically and globally;
P2: Coping with the variation of $q_j(t)$ locally;
P3: Attenuating the impact of external disturbance $w_j(t)$.

Remark 2 (Timescales)**.** The above three problems can be interpreted from the perspective of intrinsic multiple timescales in power systems. **P1** is the long-term operation problem, i.e., the system should operate economically in a steady state. **P2** is the short-term control problem, where the low-frequency variation should be eliminated by designing proper controller. The timescale of **P3** is even faster than that of **P2**, where the controller cannot track the high-frequency disturbance accurately. In this situation, we hope to attenuate its negative impact. Thus, we resolve the distributed frequency control problem under time-varying power imbalance systematically from three different timescales, which coincides with **P1-P3**.

III. Controller Design

In this section, the known steady-state part $\overline{P}_j^{in}$ is optimally balanced across all areas using a consensus-based distributed control, which resolves **P1**. Then the effect of variation part $q_j(t)$ is eliminated locally by using a supplementary internal model controller, resolving **P2**. In terms of **P3**, here we do not design a specific controller to deal with $w_j(t)$. Instead we show that the proposed controller can effective attenuate $w_j(t)$, which will be discussed in later on Section V.

A. Controller for the Known Steady-state $\bar{P}_j^{in}$

First we formulate a counterpart optimization model for the optimal load control problem:

$$\begin{aligned} \text{OLC:} \quad \min_{P_j^l} \quad & \sum_{j\in N} \frac{1}{2}\beta_j \cdot \left(P_j^l\right)^2 && \text{(9a)} \\ \text{s. t.} \quad & \textstyle\sum_{j\in N} \overline{P}_j^{in} = \sum_{j\in N} P_j^l && \text{(9b)} \end{aligned}$$

where $\beta_j > 0$ are constants. The control goal of each area is to minimize the regulation cost of the controllable load, which is in a quadratic form [18]. (9b) is the power balance constraint. Let $\tilde{q}_j(t) = 0$, we design a consensus-based controller [18]

$$\begin{aligned} P_j^l &= \mu_j/\beta_j && \text{(10a)} \\ \dot{\mu}_j &= -\textstyle\sum_{k\in N_{cj}}(\mu_j - \mu_k) + \omega_j/\beta_j && \text{(10b)} \end{aligned}$$

This simple controller can restore the frequency and minimize the regulation cost of the controllable loads when $\tilde{q}_j(t) = 0$. However, a time-varying $\tilde{q}_j(t)$ may destroy the controller. Next we use a supplementary controller to deal with $\tilde{q}_j(t)$.

B. Controller Considering Varying Power Imbalance

In this subsection, an adaptive internal model control is supplemented to mitigate $q_j(t)$, which is given by

$$\begin{aligned} P_j^l &= \mu_j/\beta_j + [d_j\omega_j + \tilde{A}_j(\hat{\alpha}_j)\zeta_j] && \text{(11a)} \\ \dot{\mu}_j &= -\textstyle\sum_{k\in N_{cj}}(\mu_j - \mu_k) + \omega_j/\beta_j && \text{(11b)} \\ \dot{\eta}_j &= -\eta_j + \overline{P}_j^{in} - P_j^l - D_j\omega_j \\ &\quad + \sum_{i:i\to j} B_{ij}(\theta_i - \theta_j) - \sum_{k:j\to k} B_{jk}(\theta_j - \theta_k) && \text{(11c)} \\ \dot{\zeta}_j &= A_j(\hat{\alpha}_j)\zeta_j - G_j(\eta_j + R_j\zeta_j) && \text{(11d)} \\ \dot{\hat{\alpha}}_j &= -k_\alpha \Lambda_j(\zeta_j)(\eta_j + R_j\zeta_j) && \text{(11e)} \end{aligned}$$

where $k_\alpha > 0, \gamma > 0$ are constant coefficients, and

$$\begin{aligned} G_j &= [\ \mathbf{0}_{1\times(\bar{s}_j-2)},\ 1,\ \gamma\ ]^T, \\ \Lambda_j(\zeta_j) &= [\ \zeta_{j2},\ \zeta_{j4},\ \cdots,\ \zeta_{j,\bar{s}_j-1}\ ]^T. \end{aligned}$$

Here, (11b) is the same as (10b), which is used to synchronize μ_j and restore frequency. Dynamics of $\eta_j, \zeta_j, \hat{\alpha}_j$ are derived from the adaptive internal model. Dynamics of η_j come from (1b) for estimating unknown $q_j(t)$. ζ_j reproduces the dynamics of φ_j in (8a). $\hat{\alpha}_j$ is the estimation of α_j.

In the controller (11a), μ_j/β_j allocates $\overline{P}_j^{in}$ economically; $\tilde{A}_j(\hat{\alpha}_j)\zeta_j$ is the output of the internal model, which is used to eliminate $q_j(t)$ asymptotically; and $d_j\omega_j$ is used to guarantee stability and enhance robustness of the controller. It is illustrated in Section VI that a low-order internal model control suffices to trace and compensate the power variation very well.

C. Closed-loop Dynamics

Combining (1) with (11) and omit $w_j(t)$, we obtain a closed-loop system. Since we are only interested in angle difference between two areas, use $\tilde{\theta}_{ij} := \theta_i - \theta_j$ as the new state variable. Then perform the following transformation

$$\begin{aligned} \tilde{\eta}_j &:= R_j\varphi_j + \eta_j \\ \tilde{\zeta}_j &:= \zeta_j - \varphi_j \\ \tilde{\alpha}_j &:= \hat{\alpha}_j - \alpha_j \end{aligned} \qquad (12)$$

Their derivatives are

$$\begin{aligned} \dot{\tilde{\eta}}_j &= R_j\dot{\varphi}_j + \dot{\eta}_j \\ &= R_jA_j(\alpha_j)\varphi_j - \eta_j + \overline{P}_j^{in} + \sum_{i:i\to j} B_{ij}\tilde{\theta}_{ij} \\ &\quad - \sum_{k:j\to k} B_{jk}\tilde{\theta}_{jk} - D_j\omega_j - \left(\mu_j/\beta_j + d_j\omega_j + \tilde{A}_j(\hat{\alpha}_j)\zeta_j\right) \\ &= R_jA_j(\alpha_j)\varphi_j - \eta_j - \tilde{A}_j(\alpha_j)\varphi_j + \tilde{A}_j(\alpha_j)\varphi_j \\ &\quad + \overline{P}_j^{in} + \sum_{i:i\to j} B_{ij}\tilde{\theta}_{ij} - \sum_{k:j\to k} B_{jk}\tilde{\theta}_{jk} \\ &\quad - D_j\omega_j - \mu_j/\beta_j - d_j\omega_j - \tilde{A}_j(\hat{\alpha}_j)\zeta_j \\ &= -\tilde{\eta}_j + \tilde{A}_j(\alpha_j)\varphi_j - \tilde{A}_j(\hat{\alpha}_j)\zeta_j + \overline{P}_j^{in} + \sum_{i:i\to j} B_{ij}\tilde{\theta}_{ij} \\ &\quad - \sum_{k:j\to k} B_{jk}\tilde{\theta}_{jk} - D_j\omega_j - \mu_j/\beta_j - d_j\omega_j && \text{(13a)} \\ \dot{\tilde{\zeta}}_j &= \dot{\zeta}_j - \dot{\varphi}_j \\ &= A_j(\hat{\alpha}_j)\zeta_j - G_j(\eta_j + R_j\zeta_j) - A_j(\alpha_j)\varphi_j \end{aligned}$$

$$
\begin{aligned}
&= (A_j(\hat{\alpha}_j) - A_j(\alpha_j))\zeta_j + A_j(\alpha_j)(\zeta_j - \varphi_j) \\
&\quad -G_j(\eta_j + R_j\zeta_j - R_j\varphi_j + R_j\varphi_j) \\
&= (A_j(\hat{\alpha}_j) - A_j(\alpha_j))\zeta_j + (A_j(\alpha_j) - G_jR_j)\tilde{\zeta}_j - G_j\tilde{\eta}_j
\end{aligned} \tag{13b}
$$

$$
\begin{aligned}
\dot{\tilde{\alpha}}_j &= \dot{\hat{\alpha}}_j - \dot{\alpha}_j \\
&= -k_\alpha \Lambda_j(\zeta_j)(\eta_j + R_j\zeta_j) \\
&= -k_\alpha \Lambda_j(\zeta_j)(\tilde{\eta}_j + R_j\tilde{\zeta}_j)
\end{aligned} \tag{13c}
$$

Define $\rho_{qj} := \tilde{A}_j(\alpha_j)\varphi_j - \tilde{A}_j(\hat{\alpha}_j)\zeta_j$. Then the closed-loop system is converted into

$$
\dot{\tilde{\theta}}_{ij} = \omega_i - \omega_j \tag{14a}
$$

$$
\begin{aligned}
\dot{\omega}_j &= \frac{1}{M_j}\Bigg(\overline{P}_j^{in} + \rho_q + \sum_{i:i\to j} B_{ij}\tilde{\theta}_{ij} - \sum_{k:j\to k} B_{jk}\tilde{\theta}_{jk} \\
&\quad -\mu_j/\beta_j - d_j\omega_j - D_j\omega_j\Bigg)
\end{aligned} \tag{14b}
$$

$$
\dot{\mu}_j = -\sum_{k\in N_{cj}}(\mu_j - \mu_k) + \omega_j/\beta_j \tag{14c}
$$

$$
\begin{aligned}
\dot{\tilde{\eta}}_j &= -\tilde{\eta}_j + \overline{P}_j^{in} + \rho_q + \sum_{i:i\to j} B_{ij}\tilde{\theta}_{ij} - \sum_{k:j\to k} B_{jk}\tilde{\theta}_{jk} \\
&\quad -D_j\omega_j - \mu_j/\beta_j - d_j\omega_j
\end{aligned} \tag{14d}
$$

$$
\dot{\tilde{\zeta}}_j = (A_j(\hat{\alpha}_j) - A_j(\alpha_j))\zeta_j + (A_j(\alpha_j) - G_jR_j)\tilde{\zeta}_j - G_j\tilde{\eta}_j \tag{14e}
$$

$$
\dot{\tilde{\alpha}}_j = -k_\alpha \Lambda_j(\zeta_j)(\tilde{\eta}_j + R_j\tilde{\zeta}_j) \tag{14f}
$$

IV. Equilibrium Point and Stability

In this section, we analyze the equilibrium and stability of the closed-loop system (14). Note that $w_j(t)$ is *not* considered.

A. Equilibrium Point

First we define the equilibrium point of the closed-loop system (14).

Definition 1. A point $(\tilde{\theta}^*, \omega^*, \mu^*, \tilde{\eta}^*, \tilde{\zeta}^*, \tilde{\alpha}^*)$ [3] is an *equilibrium point* of the closed-loop system (14) if the right-hand side of (14) vanishes at $(\tilde{\theta}^*, \omega^*, \mu^*, \tilde{\eta}^*, \tilde{\zeta}^*, \tilde{\alpha}^*)$.

The next theorem shows that two problems **P1** and **P2** are solved simultaneously at the equilibrium point.

Theorem 1. At the equilibrium point of (14), following assertions are true.

1) $\tilde{\eta}_j^* = \tilde{\zeta}_j^* = \tilde{\alpha}_j^* = 0$, which implies that $q_j(t)$ is accurately estimated.
2) System frequency recovers to the nominal value, i.e. $\omega_j^* = 0$ for all $j \in N$.
3) The marginal controllable load costs satisfy $\mu_j^* = \mu_k^*$ for all $j,k \in N$.

Proof of Theorem 1. In an equilibrium point, we have

$$
0 = \omega_i^* - \omega_j^* \tag{15a}
$$

$$
0 = \overline{P}_j^{in} + \rho_q^* + \sum_{i:i\to j} B_{ij}\tilde{\theta}_{ij}^* - \sum_{k:j\to k} B_{jk}\tilde{\theta}_{jk}^* - \frac{\mu_j^*}{\beta_j} - (d_j + D_j)\omega_j^* \tag{15b}
$$

$$
0 = -\sum_{k\in N_{cj}}(\mu_j^* - \mu_k^*) + \omega_j^*/\beta_j \tag{15c}
$$

$$
\begin{aligned}
0 &= -\tilde{\eta}_j^* + \overline{P}_j^{in} + \rho_q^* + \sum_{i:i\to j} B_{ij}\tilde{\theta}_{ij}^* - \sum_{k:j\to k} B_{jk}\tilde{\theta}_{jk}^* \\
&\quad -\mu_j^*/\beta_j - (d_j + D_j)\omega_j^*
\end{aligned} \tag{15d}
$$

$$
0 = (A_j(\hat{\alpha}_j^*) - A_j(\alpha_j))\zeta_j^* + (A_j(\alpha_j) - G_jR_j)\tilde{\zeta}_j^* - G_j\tilde{\eta}_j^* \tag{15e}
$$

$$
0 = -k_\alpha \Lambda_j(\zeta_j^*)(\tilde{\eta}_j^* + R_j\tilde{\zeta}_j^*) \tag{15f}
$$

We have $\tilde{\eta}_j^* = 0$ due to (15d) and (15b). Then (7) yields

$$
A_j(\hat{\alpha}_j^*) - A_j(\alpha_j) = \begin{bmatrix} \mathbf{0}_{2s_j\times 1} & \mathbf{0}_{2s_j} \\ 0 & \tilde{\alpha}_{j1}, 0, \cdots, \tilde{\alpha}_{js_j}, 0 \end{bmatrix} \tag{16}
$$

and

$$
\begin{aligned}
A_j(\alpha_j) - G_jR_j &= \begin{bmatrix} \mathbf{0}_{2s_j\times 1} & I_{2s_j} \\ 0 & \alpha_{j1}, 0, \cdots, \alpha_{js_j}, 0 \end{bmatrix} \\
&\quad - \begin{bmatrix} \mathbf{0} \\ 1 \\ \gamma \end{bmatrix} [r_{j1}, \cdots, r_{j,\bar{s}_j-1}, 1] \\
&= \begin{bmatrix} \mathbf{0}_{\bar{s}_j-2,1} & I_{\bar{s}_j-2} & \mathbf{0}_{\bar{s}_j-2,1} \\ -r_{j1} & -r_{j2}, \cdots, -r_{j,\bar{s}_j-1} & 0 \\ -\gamma r_{i1} & \alpha_{j1} - \gamma r_{j2}, -\gamma r_{j3}, \cdots, -\gamma r_{j,\bar{s}_j-1} & -\gamma \end{bmatrix}
\end{aligned} \tag{17}
$$

Then the first $\bar{s}_j - 1$ dimension of (15e) is rewritten as

$$
\underbrace{\begin{bmatrix} \mathbf{0}_{\bar{s}_j-2,1} & I_{\bar{s}_j-2} \\ -r_{j1} & -r_{j2}, \cdots, -r_{j,\bar{s}_j-1} \end{bmatrix}}_{\Psi} \begin{bmatrix} \tilde{\zeta}_{j1}^* \\ \vdots \\ \tilde{\zeta}_{j,\bar{s}_j-1}^* \end{bmatrix} = \mathbf{0} \tag{18}
$$

The first matrix in (18), denoted by Ψ, is nonsingular. Hence we have $\left[\tilde{\zeta}_{j1}^*, \cdots, \tilde{\zeta}_{j,\bar{s}_j-1}^*\right]^T = \mathbf{0}$. Denote $\tilde{\alpha}_j := [\tilde{\alpha}_{j1}, \cdots, \tilde{\alpha}_{j,s_j}]^T$. Then the $\bar{s}_j$-th dimension of (15e) together with (15f) yield

$$
\begin{aligned}
\Lambda_j^T(\zeta_j)\tilde{\alpha}_j^* - \gamma\tilde{\zeta}_{j,\bar{s}_j}^* &\equiv 0 \\
\Lambda_j(\zeta_j)\tilde{\zeta}_{j,\bar{s}_j}^* &\equiv \mathbf{0}
\end{aligned}
$$

This implies $\tilde{\zeta}_{j,\bar{s}_j}^* = 0$ and $\tilde{\alpha}_j^* = \mathbf{0}$. The first assertion is proved.

From the first assertion, we have

$$
\rho_{qj}^* = -\tilde{A}_j(\hat{\alpha}_j^*)\zeta_j^* + \tilde{A}_j(\alpha_j)\varphi_j = 0 \tag{19}
$$

From (15a), we have $\omega_i^* = \omega_j^* = \omega_0$, with a constant ω_0. Considering the compact form of (15c), we have

$$
-L\mu^* + \omega_0 \cdot \beta^{-1} = 0 \tag{20}
$$

where,

$$
L := \begin{bmatrix} L_1 \\ \vdots \\ L_n \end{bmatrix}, \; L_n := -(L_1 + L_2 + \cdots + L_{n-1})
$$

and L_i is the i-th row of L. Then (20) is equivalent to

$$
\begin{bmatrix} -L_1\mu^* \\ \vdots \\ -L_{n-1}\mu^* \\ (L_1 + L_2 + \cdots + L_{n-1})\mu^* \end{bmatrix} = \begin{bmatrix} -\omega_0/\beta_1 \\ -\omega_0/\beta_2 \\ \vdots \\ -\omega_0/\beta_n \end{bmatrix} \tag{21}
$$

[3] Given a collection of y_i for i in a certain set Y, y denotes the column vector $y := (y_i, i \in Y)$ of a proper dimension with y_i as its components.

Thus we have $\omega_0 = 0$, which is the second assertion.

From (20), we have $L\mu^* = 0$. Equivalently, $\mu^* = \mu_0 \cdot \mathbf{1}$ with a constant μ_0, implying the third assertion. □

From the first assertion and invoking (12), we have $\zeta_j^* = \varphi_j, \hat{\alpha}_j^* = \alpha_j$, implying the variation $q_j(t)$ is accurately eliminated. Then **P2** is solved. From the third assertion, **P1** is solved. Therefore, **P1** and **P2** are solved simultaneously.

B. Asymptotic stability

In this subsection, we prove the asymptotic stability of the closed-loop system (14). We start by transforming it to an equivalent form.

Denote $\hat{\eta}_j := \tilde{\eta}_j - M_j\omega_j$ and $\nu_j := [\hat{\eta}_j,\ \tilde{\zeta}_j,\ \tilde{\alpha}_j]^T$. Then (14) can be rewritten as

$$\begin{aligned}
\dot{\tilde{\theta}}_{ij} &= \omega_i - \omega_j && (22a)\\
\dot{\omega}_j &= \frac{1}{M_j}\Big(\overline{P}_j^{in} + \rho_{qj} + \sum_{i:i\to j} B_{ij}\tilde{\theta}_{ij} - \sum_{k:j\to k} B_{jk}\tilde{\theta}_{jk} \\
&\quad -\mu_j/\beta_j - d_j\omega_j - D_j\omega_j\Big) && (22b)\\
\dot{\mu}_j &= -\textstyle\sum_{k\in N_{cj}}(\mu_j - \mu_k) + \omega_j/\beta_j && (22c)\\
\dot{\nu}_j &= \phi_j(\nu_j, \omega_j) && (22d)
\end{aligned}$$

where

$$\phi_j(\nu_j,\omega_j) = \begin{bmatrix} -\hat{\eta}_j - M_j\omega_j \\ \begin{pmatrix} (A_j(\hat{\alpha}_j) - A_j(\alpha_j))\zeta_j - G_j(\hat{\eta}_j + M_j\omega_j) \\ +(A_j(\alpha_j) - G_jR_j)\tilde{\zeta}_j \end{pmatrix} \\ -k_\alpha\Lambda_j(\zeta_j)(\hat{\eta}_j + M_j\omega_j + R_j\tilde{\zeta}_j) \end{bmatrix}$$

It is obvious that if (14) is stable, (22) is also stable. Thus, we turn to prove the stability of (22).

Consider the subsystem ν_j , we have the following Lemma.

Lemma 2. Consider the subsystem (22d) and let $\omega_j \equiv 0$. Then for each $j \in N$, there exists a C^1 function $U_j(t,\nu_j)$ such that

$$\begin{aligned}
&\underline{U}_j(\nu_j) \le U_j(t,\nu_j) \le \overline{U}_j(\nu_j)\\
&\frac{\partial U_j(t,\nu_j)}{\partial t} + \frac{\partial U_j(t,\nu_j)}{\partial \nu_j}\phi_j(\nu_j,0) \le -\left\|\nu_j\right\|^2\\
&\left\|\frac{\partial U_j(t,\nu_j)}{\partial \nu_j}\right\| \le b_{j0}(\left\|\nu_j\right\| + \left\|\nu_j\right\|^3) \qquad (23)
\end{aligned}$$

with a constant $b_{j0} > 0$ and positive definite and radially unbounded functions $\underline{U}_j(\nu_j), \overline{U}_j(\nu_j)$.

The proof of Lemma 2 is given in [21, Lemma 3], which is omitted here.

Before giving the stability result, we first study the Euclidean norm of $\left\|\rho_{qj}\right\|$ and $\left\|\frac{\partial U_j(t,\nu_j)}{\partial \nu_j}\left(\phi_j(\nu_j,\omega_j) - \phi_j(\nu_j,0)\right)\right\|$. For ρ_{qj},

$$\begin{aligned}
\left\|\rho_{qj}\right\| &= \left\|\tilde{A}_j(\alpha_j)\varphi_j - \tilde{A}_j(\hat{\alpha}_j)(\tilde{\zeta}_j + \varphi_j)\right\|\\
&= \left\|(\tilde{A}_j(\alpha_j) - \tilde{A}_j(\hat{\alpha}_j))\varphi_j - \tilde{A}_j(\hat{\alpha}_j)\tilde{\zeta}_j\right\|\\
&= \left\|R_j\hat{A}_j(\tilde{\alpha}_j)\varphi_j - \tilde{A}_j(\tilde{\alpha}_j + \alpha_j)\tilde{\zeta}_j\right\|\\
&\le \left\|R_j\hat{A}_j(\tilde{\alpha}_j)\varphi_j\right\| + \left\|\tilde{A}_j(\tilde{\alpha}_j + \alpha_j)\tilde{\zeta}_j\right\|\\
&\le \left\|R_j\right\|\left\|\hat{A}_j(\tilde{\alpha}_j)\right\|\left\|\varphi_j\right\| + \left\|R_j\tilde{\zeta}_j + R_jA_j(\tilde{\alpha}_j + \alpha_j)\tilde{\zeta}_j\right\|\\
&= \left\|R_j\right\|\left\|\hat{A}_j(\tilde{\alpha}_j)\right\|\left\|\varphi_j\right\|\\
&\quad + \left\|R_j\tilde{\zeta}_j + R_jA_j(\alpha_j)\tilde{\zeta}_j + R_j\bar{A}_j(\tilde{\alpha}_j)\tilde{\zeta}_j\right\|\\
&\le \left\|R_j\right\|\left\|\hat{A}_j(\tilde{\alpha}_j)\right\|\left\|\varphi_j\right\|\\
&\quad + \left\|R_j\tilde{\zeta}_j\right\| + \left\|R_jA_j(\alpha_j)\tilde{\zeta}_j\right\| + \left\|R_j\bar{A}_j(\tilde{\alpha}_j)\tilde{\zeta}_j\right\|\\
&\le c_2(\left\|\nu_j\right\| + \left\|\nu_j\right\|^2) \qquad (24)
\end{aligned}$$

where

$$\begin{aligned}
\hat{A}_j(\tilde{\alpha}_j) &= \begin{bmatrix} \tilde{\alpha}_{j1} & 0 & \tilde{\alpha}_{j2} & 0 & \cdots & \tilde{\alpha}_{js_j} & 0 \end{bmatrix}\\
\bar{A}_j(\tilde{\alpha}_j) &= \begin{bmatrix} \mathbf{0}_{(\bar{s}_j-1)\times 1} & \mathbf{0}_{\bar{s}_j-1,\bar{s}_j-1} \\ \tilde{\alpha}_{j1} & 0,\tilde{\alpha}_{j2},0,\cdots,\tilde{\alpha}_{js_j},0 \end{bmatrix}\\
c_2 &\ge \left\|R_j\right\|\left\|\hat{A}_j(\tilde{\alpha}_j)\right\| + \left\|R_j\right\| + \left\|R_jA_j(\alpha_j)\right\|, \forall j \in N
\end{aligned}$$

The last "$\le$" is due to the boundedness of ϕ_j. Define a set $\Omega_\nu := \{\nu |\ \sum_{j\in N} U_j(t,\nu_j) \le \tilde{c}\}$. Since $U_j(t,\nu_j)$ is radially unbounded, there exists a constant $\bar{c}$ such that $\left\|\nu_j(t)\right\| \le \bar{c}$ for any $\nu \in \Omega_\nu$. In Ω_ν, we have

$$\left\|\rho_{qj}\right\| = \left\|\tilde{A}_j(\alpha_j)\phi_j - \tilde{A}_j(\hat{\alpha}_j)\zeta_j\right\| \le c_3\left\|\nu_j\right\| \qquad (25)$$

for a suitable $c_3 > 0$ (defined in (29)).

Similarly,

$$\begin{aligned}
\left\|\phi_j(\nu_j,\omega_j) - \phi_j(\nu_j,0)\right\| &= \left\|\begin{bmatrix} -M_j\omega_j \\ -G_jM_j\omega_j \\ -k_\alpha\Lambda_j(\zeta_j)M_j\omega_j \end{bmatrix}\right\|\\
&\le \left(\left\|M_j\right\| + \left\|G_j\right\|\left\|M_j\right\| + k_\alpha\left\|M_j\right\|\left\|\nu_j\right\|\right)\left\|\omega_j\right\|\\
&\le c_3\left\|\omega_j\right\| \qquad (26)
\end{aligned}$$

From Lemma 2, we have

$$\left\|\frac{\partial U_j(t,\nu_j)}{\partial \nu_j}\right\| \le c_3\left\|\nu_j\right\| \qquad (27)$$

Combining (26) and (27), we have

$$\begin{aligned}
&\left\|\frac{\partial U_j(t,\nu_j)}{\partial \nu_j}\left(\phi_j(\nu_j,\omega_j) - \phi_j(\nu_j,0)\right)\right\|\\
&\qquad \le \frac{1}{2}\left\|\nu_j\right\|^2 + \frac{1}{2}c_3^4\left\|\omega_j\right\|^2 \qquad (28)
\end{aligned}$$

where

$$\begin{aligned}
c_3 \ge \max\{&1,\ c_2(1+\bar{c}),\ b_{j0}(1+\bar{c}^2),\\
&\left\|M_j\right\| + \left\|G_j\right\|\left\|M_j\right\| + k_\alpha\left\|M_j\right\|\bar{c}\},\ \forall j \in N \qquad (29)
\end{aligned}$$

We give an assumption.

A1: The control parameter d_j satisfies

$$d_j > \max\left\{\frac{1+2c_3^6}{2} - D_j,\ \frac{2c_3^2+1}{4c_3^2} + \frac{2c_3^6 - c_3^4}{2c_3^2 - 2} + 2c_3^2 - D_j\right\} \qquad (30)$$

A1 is easy to satisfy by letting d_j large enough. Denote the state variables of (22) as $x = \left[\tilde{\theta}^T, \omega^T, \mu^T, \nu^T\right]^T$ and $x_1 = \left[\tilde{\theta}^T, \omega^T,\ \mu^T\right]^T$. Similar to Definition 1, we have

Definition 2. A point x^* is an *equilibrium point* of the closed-loop system (22) if the right-hand side of (22) vanishes at x^*.

Define a Lyapunov candidate function as

$$V(t,x_1,\nu) = \frac{1}{2c_3^2}V_1 + V_2 \qquad (31)$$

where

$$V_1 = \frac{1}{2}(x_1 - x_1^*)^T \Gamma (x_1 - x_1^*) \tag{32}$$

with $\Gamma := \mathrm{diag}(B, M, I_n)$,

$$V_2 = \sum\nolimits_{j\in N} U_j(t, \nu_j) \tag{33}$$

From Lemma 2 and (32), there are positive definite and radially unbounded functions $\underline{V}(x_1,\nu), \overline{V}(x_1,\nu)$ such that $\underline{V}(x_1,\nu) \le V(t,x_1,\nu) \le \overline{V}(x_1,\nu)$. Define a set $\Omega_{\overline{V}} = \left\{(x_1,\nu) | \ \overline{V}(x_1,\nu) \le \tilde{c}\right\}$. We have $\forall (x_1,\nu) \in \Omega_{\overline{V}}$, then $\nu \in \Omega_\nu$ and $\left\|\nu_j(t)\right\| \le \overline{c}$.

Finally, the stability result is given.

Theorem 3. Assume A1 holds. Then every trajectory of (22) $x(t)$ starting from $\Omega_{\overline{V}}$ converges to x^* asymptotically.

Proof of Theorem 3. Define the following function

$$h(x_1) = \begin{bmatrix} BC^T \omega \\ \overline{P}^{in} - \beta^{-1}\mu - (D+d)\omega - CB\tilde{\theta} \\ -L\mu + \beta^{-1}\omega \end{bmatrix} \tag{34}$$

The derivative of V_1 is

$$\begin{aligned} \dot{V}_1 &= (x_1 - x_1^*)^T \Gamma \cdot \dot{x}_1 \\ &= (x_1 - x_1^*)^T h(x_1) + \sum_{j\in N} \omega_j \left(\tilde{A}_j(\alpha_j)\varphi_j - \tilde{A}_j(\hat{\alpha}_j)\zeta_j\right) \end{aligned} \tag{35}$$

The first part of $\dot{V}_1$ is

$$\begin{aligned} &(x_1 - x_1^*)^T h(x_1) \\ &= \int_0^1 (x_1 - x_1^*)^T \frac{\partial}{\partial y} h(y(s))(x_1 - x_1^*) ds + (x_1 - x_1^*)^T h(x_1^*) \\ &\le \frac{1}{2}\int_0^1 (x_1 - x_1^*)^T \left[\frac{\partial^T}{\partial y} h(y(s)) + \frac{\partial}{\partial y} h(y(s))\right](x_1 - x_1^*) \mathrm{d}s \\ &= \int_0^1 (x_1 - x_1^*)^T \left[H(y(s))\right](x_1 - x_1^*) \mathrm{d}s \end{aligned} \tag{36}$$

where $y(s) = x_1^* + s(x_1 - x_1^*)$. The second equation is from the fact that $h(x_1) - h(x_1^*) = \int_0^1 \frac{\partial}{\partial y} h(y(s))(x_1 - x_1^*) \mathrm{d}s$. The inequality is due to either $h(x_1^*) = 0$ or $h(x_1^*) < 0, x_1 \ge 0$, i.e. $(x_1 - x_1^*)^T h(x_1^*) \le 0$.

$$\frac{\partial h(x_1)}{\partial x_1} = \begin{bmatrix} 0 & BC^T & 0 \\ -CB & -(D+d) & -\beta^{-1} \\ 0 & \beta^{-1} & -L \end{bmatrix} \tag{37}$$

where $D = \mathrm{diag}(D_i)$, $d = \mathrm{diag}(d_i)$, C is the incidence matrix of the communication graph.

Finally, H in (36) is

$$\begin{aligned} H &= \frac{1}{2}\left[\frac{\partial^T}{\partial x_1} h(x_1) + \frac{\partial}{\partial x_1} h(x_1)\right] \\ &= \begin{bmatrix} 0 & 0 & 0 \\ 0 & -(D+d) & 0 \\ 0 & 0 & -L \end{bmatrix} \end{aligned}$$

The second part of $\dot{V}_1$ is

$$\begin{aligned} &\sum\nolimits_{j\in N} \omega_j \left(\tilde{A}_j(\alpha_j)\phi_j - \tilde{A}_j(\hat{\alpha}_j)\zeta_j\right) \\ &\le \frac{1}{2}\|\omega\|^2 + \frac{1}{2}\sum\nolimits_{j\in N} (\tilde{A}_j(\alpha_j)\varphi_j - \tilde{A}_j(\hat{\alpha}_j)\zeta_j)^2 \\ &\le \frac{1}{2}\|\omega\|^2 + \frac{1}{2}c_3^2\|\nu\| \end{aligned} \tag{38}$$

where the last inequality is due to (25).

Thus,

$$\begin{aligned} \dot{V}_1 \le &\int_0^1 (x_1 - x_1^*)^T \left[H(y(s))\right](x_1 - x_1^*) \mathrm{d}s \\ &+ \frac{1}{2}\|\omega\|^2 + \frac{1}{2}c_3^2\|\nu\| \end{aligned} \tag{39}$$

The derivative of V_2 is

$$\begin{aligned} \dot{V}_2 &= \sum_{j\in N}\left(\frac{\partial U_j(t,\nu_j)}{\partial t} + \frac{\partial U_j(t,\nu_j)}{\partial \nu_j}\phi_j(\nu_j,\omega_j)\right) \\ &= \sum_{j\in N}\left(\frac{\partial U_j(t,\nu_j)}{\partial t} + \frac{\partial U_j(t,\nu_j)}{\partial \nu_j}\phi_j(\nu_j,\omega_j)\right) \\ &\quad + \sum_{j\in N}\left(\frac{\partial U_j(t,\nu_j)}{\partial \nu_j}\left(-\phi_j(\nu_j,0) + \phi_j(\nu_j,0)\right)\right) \\ &= \sum_{j\in N}\left(\frac{\partial U_j(t,\nu_j)}{\partial t} + \frac{\partial U_j(t,\nu_j)}{\partial \nu_j}\phi_j(\nu_j,0)\right) \\ &\quad + \sum_{j\in N}\left(\frac{\partial U_j(t,\nu_j)}{\partial \nu_j}\left(\phi_j(\nu_j,\omega_j) - \phi_j(\nu_j,0)\right)\right) \\ &\le -\|\nu\|^2 + \frac{1}{2}\|\nu\|^2 + \frac{1}{2}c_3^4\|\omega\|^2 \\ &= -\frac{1}{2}\|\nu\|^2 + \frac{1}{2}c_3^4\|\omega\|^2 \end{aligned} \tag{40}$$

where the inequality is due to Lemma 2 and (28).

In $\Omega_{\overline{V}}$, the derivative of V is

$$\begin{aligned} \dot{V} &= \frac{1}{2c_3^2}\dot{V}_1 + \dot{V}_2 \\ &\le \frac{1}{2c_3^2}\int_0^1 (x_1 - x_1^*)^T \left[H(y(s))\right](x_1 - x_1^*)\mathrm{d}s \\ &+ \frac{1}{4c_3^2}\|\omega\|^2 + \frac{1}{4c_3^2}\sum\nolimits_{j\in N}(\tilde{A}_j(\alpha_j)\phi_j - \tilde{A}_j(\hat{\alpha}_j)\zeta_j)^2 \\ &\quad -\frac{1}{2}\|\nu\|^2 + \frac{1}{2}c_3^4\|\omega\|^2 \\ &\le -\frac{1}{4}\|\nu\|^2 + \frac{1}{2c_3^2}\int_0^1 (x_1 - x_1^*)^T \left[H(y(s))\right](x_1 - x_1^*)\mathrm{d}s \\ &\quad + \frac{1 + 2c_3^6}{4c_3^2}\|\omega\|^2 \end{aligned} \tag{41}$$

Define $\tilde{H}$ as

$$\tilde{H} := \begin{bmatrix} 0 & 0 & 0 \\ 0 & -(D+d) + \frac{1+2c_3^6}{2} I_n & 0 \\ 0 & 0 & -L \end{bmatrix}$$

Then we have

$$\dot{V} \le -\frac{1}{4}\|\nu\|^2 + \frac{1}{2c_3^2}\int_0^1 (x_1 - x_1^*)^T \tilde{H} (x_1 - x_1^*)\mathrm{d}s \tag{42}$$

It is obvious that $\tilde{H} \le 0$ holds if

$$-(D+d) + \frac{1+2c_3^6}{2} I_n < 0 \tag{43}$$

where I_n is an n-dimensional identity matrix. Indeed, Assumption A1 guarantees that (43) holds.

By LaSalle's invariance principle, we can prove that the trajectory $x(t)$ converges to the largest invariant subset of

$$W_1 = \{x | \nu^* = 0, \omega = \omega^* = 0, \mu = \mu^*\}.$$

Next we will prove that the convergence is to an equilibrium point. Since $\omega = \omega^*$ are constants, $\tilde{\theta} = C^T \omega^*$ are also constants. Then by [27, Corollary 4.1], $x(t)$ will converge to its equilibrium point x^* asymptotically. □

V. Robustness Analysis

A. Robustness Against Uncertain Parameter D_j

In the controller (11), the exact value of D_j is difficult to know, or even changes at times. However, we claim that the inaccuracy of D_j does not influence both equilibrium point of the closed-loop system (14) and its stability, as we explain.

We first consider the equilibrium point. Suppose the estimation of D_j is $\hat{D}_j$ and the estimation error is $\Delta D_j := \hat{D}_j - D_j$. Usually there is $\hat{D}_j \geq 0$. Then (14d) can be rewritten as

$$\begin{aligned} \dot{\tilde{\eta}}_j &= -\tilde{\eta}_j + \overline{P}_j^{in} + \rho_{qj} + \sum_{i:i\to j} B_{ij}\tilde{\theta}_{ij} - \sum_{k:j\to k} B_{jk}\tilde{\theta}_{jk} \\ &\quad -D_j\omega_j - \Delta D_j\omega_j - \mu_j/\beta_j - d_j\omega_j \end{aligned} \tag{44}$$

Since ω_j vanishes at equilibrium, ΔD_j does not influence the equilibrium point of the closed-loop system (14a)-(14c), (44), (14e)-(14f).

Next, we discuss the stability. When ΔD_j is considered, (22d) is rewritten as

$$\dot{\nu}_j = \begin{bmatrix} -\hat{\eta}_j - (M_j + \Delta D_j)\omega_j \\ \begin{pmatrix} (A_j(\hat{\alpha}_j) - A_j(\alpha_j))\zeta_j - G_j(\hat{\eta}_j + M_j\omega_j) \\ +(A_j(\alpha_j) - G_jR_j)\tilde{\zeta}_j \end{pmatrix} \\ -k_\alpha \Lambda_j(\zeta_j)(\hat{\eta}_j + M_j\omega_j + R_j\tilde{\zeta}_j) \end{bmatrix} \tag{45}$$

Suppose $\tilde{x}(t)$ are state variables of (22a) – (22c), (45), and $\tilde{x}^*$ is an equilibrium point of $\tilde{x}(t)$.

A2: The parameter d_j satisfies (30), where c_3 is given by

$$\begin{aligned} c_3 \geq \max\big\{&1,\ c_2(1+\overline{c}),\ b_{j0}(1+\overline{c}^2), \\ &\|M_j + \Delta D_j\| + \|G_j\|\,\|M_j\| + k_\alpha \|M_j\|\,\overline{c}\big\}. \end{aligned}$$

We have the following result.

Corollary 4. Assume A2 holds, every trajectory $\tilde{x}(t)$ of (14a)-(14c), (44), (14e)-(14f) starting from $\Omega_{\overline{V}}$ converges to the equilibrium point $\tilde{x}^*$ asymptotically.

Note that one can always choose large enough d_j. Hence Corollary 4 can be easily proved following the same line of proving Theorem 3, which is omitted here due to page limit.

In summary, the unknown parameter D_j does not influence both the equilibrium point and its stability,indicating that our controller is robust against parameter uncertainty.

B. Robustness Against Unknown Disturbances $w_j(t)$

To attenuate the effect of $w_j(t)$, one needs to guarantee that, for a given constant $\gamma > 0$, the robust performance index $\|\omega_j(t)\|^2 \leq \gamma \|w_j(t)\|^2$ holds. [28, Chapter 16], [29], [30]. It means that, for a bounded external disturbance $w_j(t)$, the frequency deviation is always bounded by the given γ. A smaller γ results in a better attenuation performance. The lower bound of γ (if it exists) is referred to as L_2 gain of the system.

When considering $w_j(t)$, the closed-loop system is

$$\dot{\tilde{\theta}}_{ij} = \omega_i - \omega_j \tag{46a}$$

$$\begin{aligned} \dot{\omega}_j = \frac{1}{M_j}\Big(&\overline{P}_j^{in} + w_j(t) + \rho_{qj} + \sum_{i:i\to j} B_{ij}\tilde{\theta}_{ij} - \sum_{k:j\to k} B_{jk}\tilde{\theta}_{jk} \\ &-\mu_j/\beta_j - d_j\omega_j - D_j\omega_j\Big) \end{aligned} \tag{46b}$$

$$\dot{\mu}_j = -\textstyle\sum_{k\in N_{cj}}(\mu_j - \mu_k) + \omega_j/\beta_j \tag{46c}$$

$$\dot{\nu}_j = \tilde{\phi}_j(\nu_j, \omega_j, w_j) \tag{46d}$$

where

$$\tilde{\phi}_j = \begin{bmatrix} -\hat{\eta}_j - M_j\omega_j - w_j(t) \\ \begin{pmatrix} (A_j(\hat{\alpha}_j) - A_j(\alpha_j))\zeta_j - G_j(\hat{\eta}_j + M_j\omega_j) \\ +(A_j(\alpha_j) - G_jR_j)\tilde{\zeta}_j \end{pmatrix} \\ -k_\alpha \Lambda_j(\zeta_j)(\hat{\eta}_j + M_j\omega_j + R_j\tilde{\zeta}_j) \end{bmatrix}.$$

By the similar analysis to (26), we have

$$\|\phi_j(\nu_j, \omega_j, w_j) - \phi_j(\nu_j, 0, 0)\| \leq c_3\|\omega_j\| + \|w_j\| \tag{47}$$

where c_3 is same as that in (29). Then

$$\begin{aligned} &\left\|\frac{\partial U_j(t,\nu_j)}{\partial \nu_j}\left(\phi_j(\nu_j, \omega_j, w_j) - \phi_j(\nu_j, 0, 0)\right)\right\| \\ &\qquad \leq \frac{1}{2}\|\nu_j\|^2 + \frac{2c_3^6 - c_3^4}{2c_3^2 - 2}\|\omega_j\|^2 + \frac{1}{2}\|w_j\|^2 \end{aligned} \tag{48}$$

Using V_1, V_2 defined in (32) and (33) again, we have

$$\begin{aligned} \dot{V}_1 \leq &\int_0^1 (x_1 - x_1^*)^T [H(y(s))](x_1 - x_1^*)\mathrm{d}s + \frac{1}{2}c_3^2\|\nu\|^2 \\ &+\frac{1}{2}\|\omega\|^2 + \frac{1}{4c_3^2}\|\omega\|^2 + c_3^2\|w\|^2 \end{aligned} \tag{49}$$

and

$$\begin{aligned} \dot{V}_2 &\leq -\|\nu\|^2 + \frac{1}{2}\|\nu_j\|^2 + \frac{2c_3^6 - c_3^4}{2c_3^2 - 2}\|\omega\|^2 + \frac{1}{2}\|w\|^2 \\ &= -\frac{1}{2}\|\nu\|^2 + \frac{2c_3^6 - c_3^4}{2c_3^2 - 2}\|\omega\|^2 + \frac{1}{2}\|w\|^2 \end{aligned} \tag{50}$$

Using the same Lyapunov function as in (31) gives

$$\begin{aligned} \dot{V} \leq &-\frac{1}{4}\|\nu\|^2 - \frac{1}{2c_3^2}(\mu - \mu^*)^T L(\mu - \mu^*) + \|w\|^2 \\ &-\frac{1}{2c_3^2}\omega^T\left(D + d - \frac{2c_3^2 + 1}{4c_3^2}I_n - \frac{2c_3^6 - c_3^4}{2c_3^2 - 2}I_n\right)\omega \end{aligned} \tag{51}$$

Thus, we have

$$\|\omega_j\|^2 \leq \gamma\|w_j\|^2 \tag{52}$$

where

$$\frac{1}{\gamma} = \min\left\{\frac{1}{2c_3^2}\left(D_j + d_j - \frac{2c_3^2 + 1}{4c_3^2} - \frac{2c_3^6 - c_3^4}{2c_3^2 - 2}\right)\right\},\ \forall j \in N \tag{53}$$

We have $\frac{1}{\gamma} > 1$ due to Assumption A1.

Inequalities (52) and (53) indicate that the controller is robust to $w_j(t)$ with the L_2-gain $\gamma < 1$. In practice, the amplitudes of $w_j(t)$ are usually quite small. As a consequence,

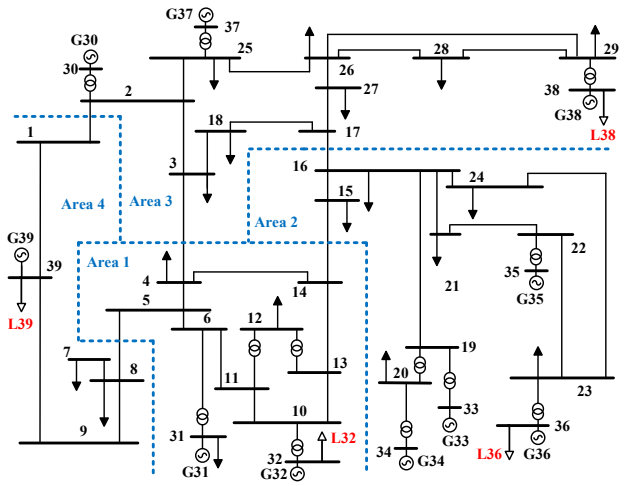

Fig. 1: The New England 39-bus system

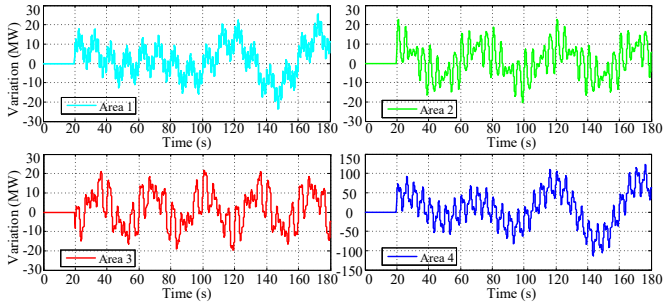

Fig. 2: Power variation of renewable resources in each area

the deviation of ω_j is also small. According to (53), a larger d_j is helpful to enhance the attenuation performance.

The analysis above shows that the controller is robust in terms of uncertain parameter D_j and unknown disturbance $w_j(t)$. Hence **P3** is resolved.

VI. Case Studies

A. System Configuration

To verify the performance of the proposed controller, the New England 39-bus system with 10 generators as shown in Fig.1 is used for test. All simulations are implemented in the commercial power system simulation software PSCAD [31].

We add four (aggregate) controllable loads to the system by connecting them at buses 32, 36, 38 and 39, respectively. Their initial values are set as (74.1, 52.7, 52.7, 105.4) MW. Then the system is divided into four control areas, as shown in Fig.1. Each area contains a controllable load. Parameters β in each area are (1, 0.8, 0.8, 0.4). The communication graph is undirected and set as $L32 \leftrightarrow L36 \leftrightarrow L38 \leftrightarrow L39 \leftrightarrow L32$. The varying power in each area is shown in Fig.2. Note that the functions of the four curves in Fig.2 are unknown to the controllers. In the controller design, we choose $s_j = 3$ in (3). Note that this does not mean the actual power variation (curves in Fig.2) are superposition of only three sinusoidal functions.

In our tests, two scenarios are studied: 1) only unknown time-varying part is considered, i.e., $\overline{P}_j^{in} = 0,\ \tilde{q}_j(t) \neq 0$; 2) both known steady-state and unknown time-varying parts are considered, i.e., $\overline{P}_j^{in} \neq 0,\ \tilde{q}_j(t) \neq 0$.

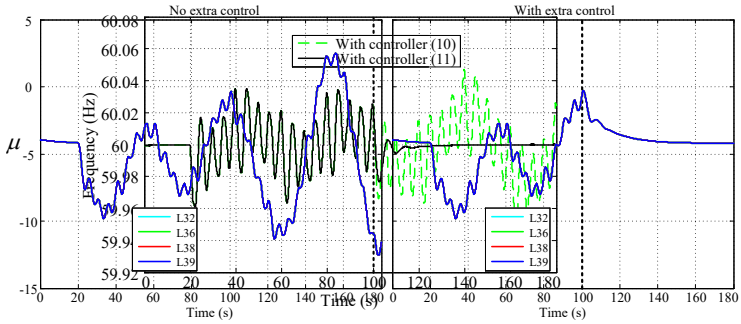

Fig. 3: System frequencies under two controls

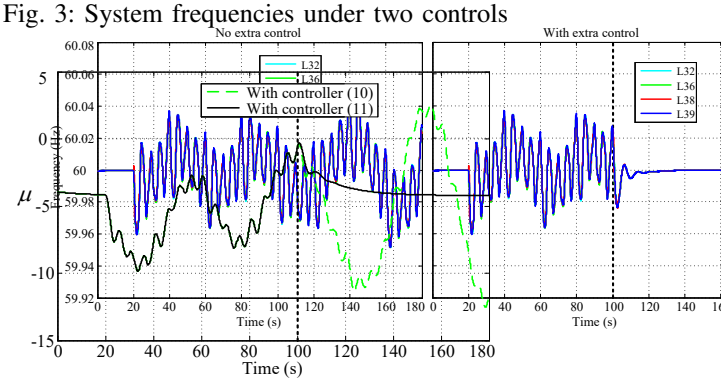

Fig. 4: Dynamics of μ under two controls

B. Scenario 1: $\overline{P}_j^{in} = 0,\ \tilde{q}_j(t) \neq 0$

In this scenario, the system operates initially in a steady state and the frequency controller (10) is adopted. At $t = 20$s, unknown power variation $\tilde{q}_j(t)$ is enforced. At $t = 100s$, the controller is switched to our controller (11). The system frequency dynamics are shown in Fig.3.

In Fig.3, the dotted green line stands for the frequency dynamics using controller (10). It is observed the frequency experiences fierce oscillation in this situation. The maximal amplitude is up to 0.05Hz. However, when controller (11) is applied at $t = 100$s, the frequency is stabilized rapidly (the black solid line). This validates the efficacy of our controller.

The dynamics of μ_j are shown in Fig.4. μ_j varies greatly before using (11), while is stabilized when (11) is activated.

The control input generated by the internal models, i.e., $\tilde{A}_j(\hat{\alpha}_j)\zeta_j$, and the actual power variations $\tilde{q}_j(t)$ in each area are compared in Fig.5. It is observed that $\tilde{A}_j(\hat{\alpha}_j)\zeta_j$ tracks $\tilde{q}_j(t)$ with high accuracy.

Moreover, we also illustrate the error between variation and internal model output, which is shown in Fig.6. It is shown that the error is very small. The error in area 4 is bigger than others, as the disturbance in area 4 is much larger than that in other areas (see Fig.2).

To demonstrate it more clearly, we define an error index Err_j as below.

$$Err_j := \frac{\int_{t_0}^{t_1} \sqrt{\left(\tilde{A}_j(\hat{\alpha}_j)\zeta_j - \tilde{q}_j(t)\right)^2}\mathrm{d}t}{\int_{t_0}^{t_1} \sqrt{(\tilde{q}_j(t))^2}\mathrm{d}t} \tag{54}$$

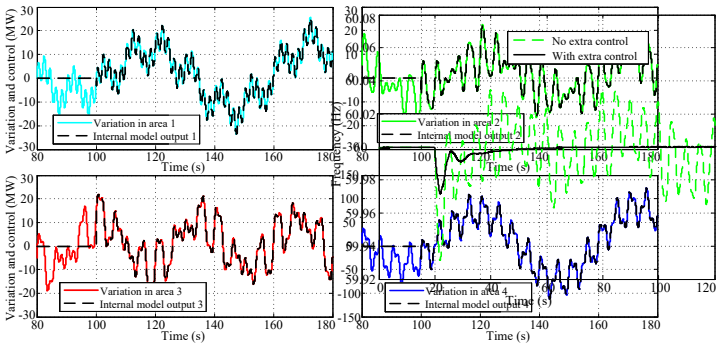

Fig. 5: Power variations and outputs of the extra controllers

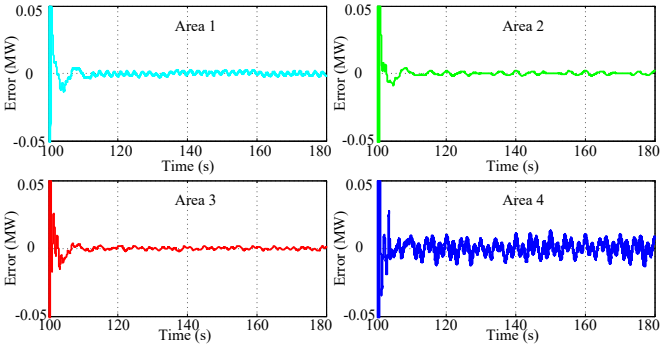

Fig. 6: Tracking errors of the extra controllers in each area

In this scenario, $t_0 = 100$, $t_1 = 180$. Err_j in each area are $(0.00042,\ 0.00075,\ 0.00091,\ 0.00040)$, all of which are very small. This result indicates that the effect of unknown power variations is almost completely mitigated.

C. Scenario 2: $\overline{P}_j^{in} \neq 0,\ q_j(t) \neq 0$

In this subsection, $\overline{P}_j^{in}$ in each area are $(15,\ 15,\ 15,\ 15)$ MW, which are the prediction of aggregated load. It should be pointed out that the prediction is not accurate. The offset errors are $(1,\ 1,\ 1,\ 5)$ MW, which are relatively small but unknown. We compare the performances using controller (10) and (11). Both the two controllers are applied at $t = 20$s. The system frequencies are compared in Fig.7.

The green line stands for the frequency dynamics using (10). The frequency oscillation is fierce and nadir is quite low. The black line stands for frequency dynamics using (11). In this situation, the nominal frequency is recovered fast without oscillation. The frequency nadir is much higher than that using (10). This result confirms that our controller can still work well when $\overline{P}_j^{in} \neq 0$.

The dynamics of μ_j are given in the left part of Fig.8. The green line stands for μ_j using (10), while the black line stands for that using (11). μ_j of each area converges to a same value, which implies the optimality is achieved, i.e., $\overline{P}_j^{in}$ is balanced economically.

In this scenario, the controllable load in each area is also composed of two parts: a steady part to balance $\overline{P}_j^{in}$ and a variation part to mitigate the effects of $\tilde{q}_j(t)$. The steady part of controllable load is given in the right part of Fig.8. The controllable loads in the steady state are $(63.8,\ 39.8,\ 39.8,\ 79.6)$ MW. The result is the same as that obtained using CVX to solve the optimization counterpart (i.e., OLC problem (9)).

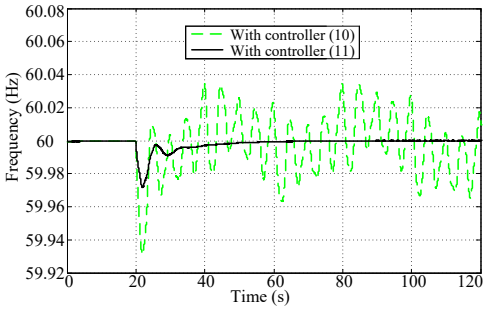

Fig. 7: System frequencies under two controls

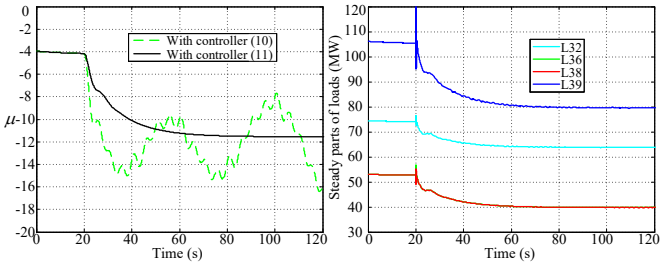

Fig. 8: Dynamics of μ and steady parts of controllable loads

The performance of controllable load tracking power variation in each area is given in Fig.9. We can find that the controllable loads coincide to the power variations with high accuracy. Again, the error index Err_j with $t_0 = 20$ and $t_1 = 120$ in this situation are $(0.0084,\ 0.0026,\ 0.0057,\ 0.0019)$, which are also very small.

D. Performance under Unknown Disturbances

To test the performance of our controller under high-frequency unknown disturbances, we add random noise $\tilde{w}(t)$ on $\tilde{q}(t)$ into the testing system, which takes the form of

$$\tilde{w}(t) = \begin{bmatrix} 10 \times \text{rand}(t) \\ 10 \times \text{rand}(t) \\ 10 \times \text{rand}(t) \\ 100 \times \text{rand}(t) \end{bmatrix} \text{MW}$$

where rand(t) is a function generating a random number between $[0,\ 1]$ at time t. The load control command and the power variations are given Fig.10. As the frequency of external disturbance is quite high, the internal model control is not able to follow it accurately. As a consequence, there exist obvious tracking errors, as shown in Fig.11. The system frequency is shown in Fig.12. The inset zooms into the frequency dynamics between 140s-160s, when the system converges to the steady state. The maximal frequency deviation is smaller than 0.001Hz, demonstrating that the unknown disturbance is well attenuated by the proposed controller.

VII. Conclusion

In this paper, we address the frequency control problem in power systems with high-penetration renewable generation

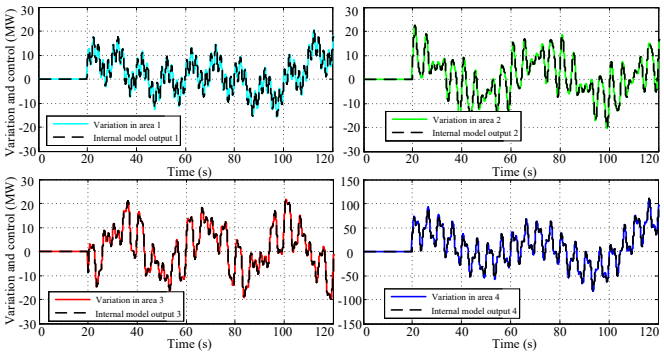

Fig. 9: Variation and internal model output with load increases

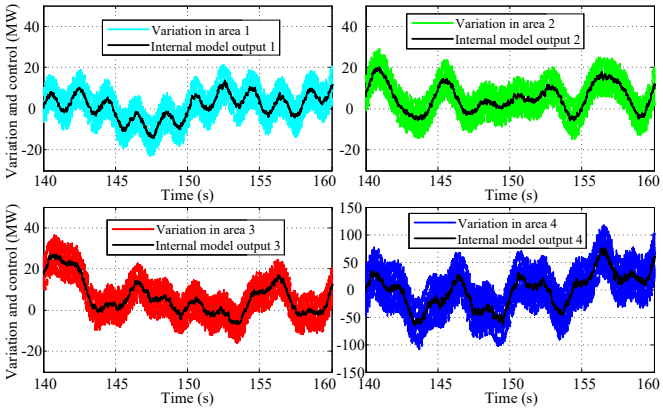

Fig. 10: Variation and internal model output with noise

integrated. We have decomposed power imbalance into three parts: the known steady part, the unknown low-frequency variation part and the unknown high-frequency residual. Then the distributed frequency control problem for the three different time scales are fitted into a same control framework, resolving the following problems:

1) **Slow timescale:** designing the consensus-based distributed control to allocate the steady part of power imbalance economically;
2) **Medium timescale:** devising an internal model control to accurately track and compensate time-varying unknown power imbalance locally;
3) **Fast timescale:** using the L_2 gain inequality to show the robustness of the controller against uncertain disturbances and parameters.

Empirical results of tests carried on the New England system confirm the efficacy of our controller.

REFERENCES

[1] L. Min and A. Abur, "Total transfer capability computation for multi-area power systems," *IEEE Trans. Power Syst.*, vol. 21, no. 3, pp. 1141–1147, Aug. 2006.

[2] A. Ahmadi-Khatir, M. Bozorg, and R. Cherkaoui, "Probabilistic spinning reserve provision model in multi-control zone power system," *IEEE Trans. Power Syst.*, vol. 28, no. 3, pp. 2819–2829, Mar. 2013.

[3] P. Kundur, *Power System Stability and Control*. McGraw-hill New York, 1994, vol. 7.

[4] F. Dörfler, J. W. Simpson-Porco, and F. Bullo, "Breaking the hierarchy: Distributed control and economic optimality in microgrids," *IEEE Trans. Control Network Syst.*, vol. 3, no. 3, pp. 241–253, 2016.

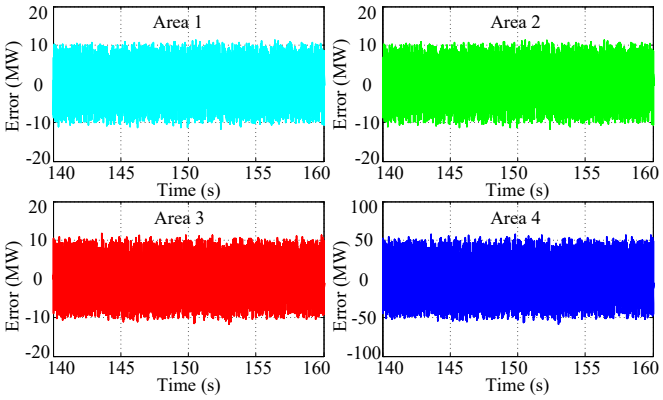

Fig. 11: Error between variation and internal model output

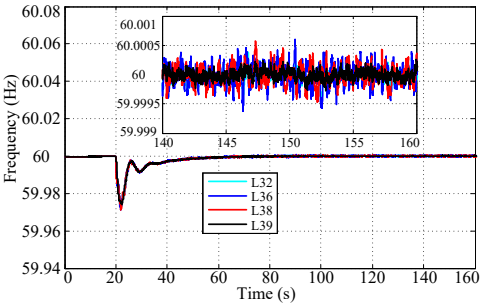

Fig. 12: Frequency under external noise

[5] F. C. Schweppe, R. D. Tabors, J. L. Kirtley, H. R. Outhred, F. H. Pickel, and A. J. Cox, "Homeostatic utility control," *IEEE Trans. Power Apparatus Syst.*, vol. PAS-99, no. 3, pp. 1151–1163, May 1980.

[6] C. Zhao, U. Topcu, N. Li, and S. H.Low., "Design and stability of load-side primary frequency control in power systems," *IEEE Trans. Autom. Control*, vol. 59, no. 5, pp. 1177–1189, Jan. 2014.

[7] A. Jokić, M. Lazar, and P. P. van den Bosch, "Real-time control of power systems using nodal prices," *Int. J. Elect. Power Energy Syst.*, vol. 31, no. 9, pp. 522–530, 2009.

[8] X. Zhang and A. Papachristodoulou, "A real-time control framework for smart power networks: Design methodology and stability," *Automatica*, vol. 58, pp. 43–50, 2015.

[9] T. Stegink, C. De Persis, and A. van der Schaft, "A unifying energy-based approach to stability of power grids with market dynamics," *IEEE Trans. Autom. Control*, vol. 62, no. 6, pp. 2612–2622, 2017.

[10] N. Li, C. Zhao, and L. Chen, "Connecting automatic generation control and economic dispatch from an optimization view," *IEEE Trans. Control Network Syst.*, vol. 3, no. 3, pp. 254–264, 2016.

[11] D. Cai, E. Mallada, and A. Wierman, "Distributed optimization decomposition for joint economic dispatch and frequency regulation," *IEEE Trans. Power Syst., early access*, 2017.

[12] E. Mallada, C. Zhao, and S. H. Low, "Optimal load-side control for frequency regulation in smart grids," *IEEE Trans. Autom. Control, to appear*, 2017.

[13] Z. Wang, F. Liu, J. Z. Pang, S. Low, and S. Mei, "Distributed optimal frequency control considering a nonlinear network-preserving model," *arXiv preprint arXiv:1709.01543*, 2017.

[14] A. Kasis, E. Devane, C. Spanias, and I. Lestas, "Primary frequency regulation with load-side participation part i: stability and optimality," *IEEE Trans. Power Syst. early access*, 2016.

[15] Z. Wang, F. Liu, S. H. Low, C. Zhao, and S. Mei, "Distributed frequency control with operational constraints, part i: Per-node power balance," *IEEE Trans. Smart Grid, in press*, 2017.

[16] ——, "Distributed frequency control with operational constraints, part ii: Network power balance," *IEEE Trans. Smart Grid, in press*, 2017.

[17] L. Y. Lu, H. J. Liu, and H. Zhu, "Distributed secondary control for isolated microgrids under malicious attacks," in *2016 North American Power Symposium (NAPS)*, Sept 2016, pp. 1–6.

[18] S. Trip, M. Bürger, and C. De Persis, "An internal model approach

to (optimal) frequency regulation in power grids with time-varying voltages," *Automatica*, vol. 64, pp. 240–253, 2016.
[19] K. Xi, H. X. Lin, and J. H. van Schuppen, "Power-imbalance allocation control of power systems – a frequency bound for time-varying loads," in *2017 36th Chinese Control Conference (CCC)*, July 2017, pp. 10 528–10 533.
[20] E. Weitenberg, Y. Jiang, C. Zhao, E. Mallada, C. De Persis, and F. Dörfler, "Robust decentralized secondary frequency control in power systems: Merits and trade-offs," *arXiv preprint arXiv:1711.07332*, 2017.
[21] X. Wang, Y. Hong, P. Yi, H. Ji, and Y. Kang, "Distributed optimization design of continuous-time multiagent systems with unknown-frequency disturbances," *IEEE Trans. Cybern.*, vol. 47, no. 8, pp. 2058–2066, Aug 2017.
[22] P. Milan, M. Wächter, and J. Peinke, "Turbulent character of wind energy," *Phys. Rev. Lett.*, vol. 110, p. 138701, Mar 2013.
[23] A. Bušiā and S. Meyn, "Distributed randomized control for demand dispatch," in *Decision and Control (CDC), 2016 IEEE 55th Conference on*. IEEE, 2016, pp. 6964–6971.
[24] L. A. Aguirre, D. D. Rodrigues, S. T. Lima, and C. B. Martinez, "Dynamical prediction and pattern mapping in short-term load forecasting," *Int. J. Electr. Power Energy Syst.*, vol. 30, no. 1, pp. 73 – 82, 2008.
[25] G. Obregon-Pulido, B. Castillo-Toledo, and A. Loukianov, "A globally convergent estimator for n-frequencies," *IEEE Trans. Automat. Contr.*, vol. 47, no. 5, pp. 857–863, May 2002.
[26] D. Xu, X. Wang, and Z. Chen, "Output regulation of nonlinear output feedback systems with exponential parameter convergence," *Syst. Control Lett.*, vol. 88, pp. 81 – 90, 2016.
[27] H. K. Khalil, *Nonlinear systems*. Prentice hall New Jersey, 1996, vol. 3.
[28] K. Zhou, J. C. Doyle, and K. Glover, *Robust and optimal control*. Prentice hall New Jersey, 1996, vol. 40.
[29] B. Qin, X. Zhang, J. Ma, S. Deng, S. Mei, and D. J. Hill, "Input to state stability based control of doubly fed wind generator," *IEEE Trans. Power Syst.*, vol. PP, no. 99, pp. 1–1, 2017.
[30] H. N. Wu and H. D. Wang, "Distributed consensus observers-based h_∞ control of dissipative pde systems using sensor networks," *IEEE Trans. Control Network Syst.*, vol. 2, no. 2, pp. 112–121, June 2015.
[31] "Home of pscad," https://hvdc.ca/pscad/, December 2017.